

Research Articles: Systems/Circuits

Population receptive field shapes in early visual cortex are nearly circular

<https://doi.org/10.1523/JNEUROSCI.3052-20.2021>

Cite as: J. Neurosci 2021; 10.1523/JNEUROSCI.3052-20.2021

Received: 3 December 2020

Revised: 3 January 2021

Accepted: 10 January 2021

This Early Release article has been peer-reviewed and accepted, but has not been through the composition and copyediting processes. The final version may differ slightly in style or formatting and will contain links to any extended data.

Alerts: Sign up at www.jneurosci.org/alerts to receive customized email alerts when the fully formatted version of this article is published.

1 Population receptive field shapes in early
2 visual cortex are nearly circular

3
4 **Abbreviated title:** Circular vs elliptical pRFs
5
6
7
8
9
10

11
12 **Authors:** Garikoitz Lerma-Usabiaga^{1,2,3}, Jonathan Winawer⁴, Brian A. Wandell^{1,2}
13

14 **Affiliation:**

15 ¹ Department of Psychology, Stanford University, 450 Serra Mall, Jordan Hall Building, 94305
16 Stanford, California, USA

17 ² Wu Tsai Neurosciences Institute, Stanford University, 94305 Stanford, California, USA

18 ³ BCBL. Basque Center on Cognition, Brain and Language. Mikeletegi Pasealekua 69, Donostia
19 - San Sebastián, 20009 Gipuzkoa, Spain

20 ⁴ Department of Psychology and Center for Neural Science, New York University, 6
21 Washington Pl, New York, NY, 10003, USA
22

23 **Corresponding Author:** Email: garikoitz@gmail.com (GLU)
24

25 **Number of pages:** 23

26 **Number of figures:** 7

27 **Number of words:** Abstract (246), Introduction (539), Discussion (1022)
28

29 **Conflicts of interest:**

30 The authors declare no competing financial interests.
31

32 **Acknowledgements:**

33 This project has received funding from the European Union's Horizon 2020 research and innovation
34 programme under the Marie Skłodowska-Curie grant agreement No 795807 to G.L.-U. and NIH grants
35 supporting J.W. (EY027401, EY027964, MH111417). While writing this paper we have been in contact
36 with E. Silson, C. Baker, and R. Reynolds. We thank R. Reynolds for help with the AFNI software.
37

38 **Keywords:** visual cortex; population receptive field; fMRI
39
40
41

42 **Abstract**

43 The visual field region where a stimulus evokes a neural response is called the receptive field (RF).
44 Analytical tools combined with functional MRI can estimate the receptive field of the population of
45 neurons within a voxel. Circular population RF (pRF) methods accurately specify the central position of
46 the pRF and provide some information about the spatial extent (diameter) of the receptive field. A number
47 of investigators developed methods to further estimate the shape of the pRF, for example whether the
48 shape is more circular or elliptical. There is a report that there are many pRFs with highly elliptical pRFs
49 in early visual cortex (V1-V3; Silson et al., 2018). Large aspect ratios (>2) are difficult to reconcile with
50 the spatial scale of orientation columns or visual field map properties in early visual cortex. We started to
51 replicate the experiments and found that the software used in the publication does not accurately estimate
52 RF shape: it produces elliptical fits to circular ground-truth data. We analyzed an independent data set
53 with a different software package that was validated over a specific range of measurement conditions, to
54 show that in early visual cortex the aspect ratios are less than 2. Furthermore, current empirical and
55 theoretical methods do not have enough precision to discriminate ellipses with aspect ratios of 1.5 from
56 circles. Through simulation we identify methods for improving sensitivity that may estimate ellipses with
57 smaller aspect ratios. The results we present are quantitatively consistent with prior assessments using
58 other methodologies.

59

60 **Significance Statement**

61 We evaluated whether the shape of many population receptive fields in early visual cortex is elliptical and
62 differs substantially from circular. We evaluated two tools for estimating elliptical models of the pRF; one
63 tool was valid over the measured compliance range. Using the validated tool, we found no evidence that

64 confidently rejects circular fits to the pRF in visual field maps V1, V2 and V3. The new measurements
65 and analyses are consistent with prior theoretical and experimental assessments in the literature.

66 Introduction

67 Small regions of the primate visual cortex (V1-V3) contain neurons whose spatial receptive fields are
68 compact and often overlap in the visual field. The receptive fields of individual neurons can be measured
69 from electrical activity (Hubel and Wiesel, 1968). Using fMRI responses, it is possible to measure the
70 receptive fields of individual cortical voxels (Dumoulin and Wandell, 2008). These fMRI responses
71 reflect the activity of many ($\sim 10^5$) neurons and are called the population receptive field (pRF). There has
72 been extensive work using pRF methods to measure visual cortex in the living human brain (Wandell and
73 Winawer, 2015) and versions of these methods with intrinsic and calcium imaging have been used in
74 animal model systems (Kalatsky and Stryker, 2003; Nauhaus et al., 2016).

75
76 The population RF estimates depend upon models of the physiological response. The early pRF models
77 used simple linear models of the physiological response, often assuming that the pRF has a canonical
78 spatial profile (e.g., circularly symmetric Gaussian; Dumoulin and Wandell, 2008). Such simple models
79 can accurately predict the fMRI time series of voxels in early visual cortex (e.g., V1-V3) when using a
80 limited range of stimuli, capturing a very large proportion of the explainable variance. Over time
81 investigators have expanded the scope of the stimuli and this required increasing the complexity of the
82 pRF models (Zuiderbaan et al., 2012; Kay et al., 2013; Greene et al., 2014; Alvarez et al., 2015).

83
84 This journal published a provocative claim that prior investigators had missed an important aspect of the
85 human population receptive field shapes in V1-V3 (Silson et al., 2018). Nearly all the prior work in which
86 a parametric form was assumed treated the pRF spatial profile as approximately circular. This question
87 had been tested, for example, by Zeidman et al. (2018), who found that elliptical fits are not better than

Circular vs elliptical pRFs

88 circular models. On the other hand, Silson et al. (2018) report that pRFs are significantly elongated, often
89 with an aspect ratio (ratio of long to short axis) of 2.5 or greater. Groups using a broader class of
90 allowable shapes have reported inconclusive results, for example finding most pRFs in V1-V3 to be
91 nearly circular but a small percentage to be quite elongated (Greene et al., 2014), or finding many voxels
92 to be slightly elongated (Merkel et al., 2018, 2020).

93

94 We set out to investigate the discrepancy between the high ellipticity report and the more common
95 assumption of near circularity by replicating the findings. We began the replication by using the same
96 software as in Silson et al. (2018). As part of our workflow, we ran the software through a recently
97 developed validation framework (Lerma-Usabiaga et al., 2020). This assessment revealed that the
98 software returns inaccurate estimates, including ellipses with aspect ratios larger than 2 when tested with
99 ground-truth circular data (aspect ratio of 1). To pursue the key scientific question, we decided to use a
100 different software tool and to perform a full assessment of how accurately this tool might measure
101 deviations from circularity. The validation of the second software tool identified a range of conditions
102 where performance is reliable. Using the validated software with retinotopy data from the 7T Human
103 Connectome Project, we find no support for a shape that is substantially and systematically different from
104 circular.

105

106

107 **Materials and Methods**

108 For software validation we used synthetic data generated using the validation framework (pRF-synthesis)
109 described by Lerma-Usabiaga et al. (2020). These methods are described in detail in that paper and
110 summarized briefly here. We added two levels of noise (low- and mid-noise) created with realistic models
111 of several noise sources, including physiological noise (cardiac and respiratory), low frequency drift, and
112 instrumental noise (white noise) derived from experimental measurements. We used bars with contrast
113 patterns that swept the 20-degree diameter visual field vertically, horizontally and in 45 and -45 degrees,
114 in two different directions each (8 bar sweeps in total). The total stimulus duration and TR (sampling rate)
115 were varied across several simulations. See Table 1 for details.

116

117 For assessing deviations from circularity of population receptive fields, we used empirical measurements
118 from the 7T HCP Retinotopy project (Benson et al., 2018). Specifically, we selected retinotopy data
119 collected from the three representative subjects analyzed in Figure 7 of that paper (HCP IDs 164131,
120 115017, and 536647). We analyzed the empirical data using the containers (pRF-analyze) described,
121 implemented, and shared by Lerma-Usabiaga et al., (2020).

122 **Experimental design and statistical analyses**

123 We evaluated the mrVista (<https://github.com/vistalab/vistasoft>) and AFNI (Cox, 1996) estimates of
124 elliptical population receptive fields. The latter was introduced in (Silson et al., 2018). The former is part
125 of the mrVista toolbox but has not previously been used in published work.

126

127 In mid-2018 the AFNI development team discovered an error in the ellipse formula. Silson et al. (2018)
128 re-ran the analyses and reported some numerical differences but no changes to the pattern of results or the

129 conclusions: the pRF solutions remained highly elongated after correcting the code. Here, we used the
 130 new, corrected version of the software. The April 4th, 2020 version is implemented in the Docker
 131 container. The noiseless analyses in Figures 1 and 2 were performed in a local macOS binary installation
 132 with an August 28th, 2018 version of Afni. We validated the corrected algorithms using synthetic (ground-
 133 truth) input data and estimated the following parameters.

- 134 • The center position of the population receptive field (x, y).
- 135 • The standard deviations (σ_1, σ_2) of the two axes of the ellipse ($\sigma_1 > \sigma_2$). (Circular fits are
 136 constrained to $\sigma_1 = \sigma_2$ and one parameter is returned.)
- 137 • The angle θ of the main axis (larger sigma). Not returned for the circular fit.
- 138 • The gain parameter A.

139 We estimated deviations from circular pRFs using the mrVista prf-Analyze container and measurements
 140 obtained from the HCP project. The prf-Analyze-mrVista container returns the distribution of aspect
 141 ratio estimates (σ_1/σ_2). We compared median values and distributions from fitting the empirical
 142 measurements with values expected from analyzing ground-truth data generated using prf-Synthesize.
 143 Several analyses were performed in this manuscript using synthetic or real data with the following
 144 parameters:

Type	Simulated or real TR (sec)	Duration (sec)	Noise	Aspect ratio	Eccentricity (deg)	pRF Size (deg)	pRF-Analysis*
Synthetic	2	400	None	{1,2}	{1,2,3,4,5,6,7,8,9}	{.5, 1,1.5,2,3,4}	{AFNI6, Vista6}
	2	400	{low,mid}	{1,2}	{1,2,3,4,5,6,7,8,9}	{0.25:0.25:6}	{AFNI6, Vista6}
	1	{300,400}	{low,mid}	{1,2}	{1,2,3,4,5,6,7,8,9}	{0.25:0.25:6}	{Vista6}
Experimental (V1,V2,V3)	1	300	NA	NA	Limited to: [2,6]	Limited to: [1,3]	{Vista6, Vista4}

145 Table 1. Main parameters of the experiments

146 * Note: 6 refers to the elliptical fits with 6 parameters, and 4 to the circular fits with 4 parameters.

147

148 Code availability and reproducibility

149 To reproduce the computations in this paper requires that Matlab and Docker be installed on your
150 computer. The configuration files and the HCP data for the empirical analyses are curated and stored in a
151 project at the Open Science Foundation (<https://osf.io/9jhcm/>). The software we describe downloads the
152 data from that OSF project.

153

154 The code specific to this paper is shared in the GitHub repository PRFmodel that is within the vistalab
155 project (<https://github.com/vistalab/PRFmodel.git>). After cloning that repository, please select the git tag
156 EllipsePaperv02. Place this repository on your Matlab path. The script pmMainEllipseFiguresScript.m
157 describes how to install the necessary support libraries and execute the relevant scripts.

158

159 The software for the pRF-Validation framework (Lerma-Usabiaga et al., 2020), including the code used
160 to synthesize the BOLD time series, is shared in the same repository. The Docker container image can be
161 downloaded from Docker hub with the command `docker pull garikoitz/prfsynth`. The mrVista analysis
162 code is publicly shared in github.com/vistalab/vistasoft, and its container can be downloaded from Docker
163 hub with the command `docker pull garikoitz/prfanalyze-vista`. The AFNI analysis code is publicly shared
164 in github.com/afni/afni, and our containerized version used for the analyses in this paper can be
165 downloaded from Docker hub with the command `docker pull garikoitz/prfanalyze-afni`.

166 Results

167 We present results about algorithm validity in noise-free and simulated noise conditions. We then define
168 a range of parameters in which one algorithm performs acceptably, and we analyze empirical
169 measurements from that range. In previous work we reported that pRF algorithms systematically
170 misestimate pRF parameters if there is a mismatch between the hemodynamic response function (HRF)

171 used to simulate the time series with the HRF assumed in the analysis tool. Throughout the simulations
172 here, we used synthetic data that matched the expected HRF.

173 Algorithm validity: noise-free analyses

174 We first set out to validate elliptical models in AFNI (“AFNI-elliptical”) and mrVista (“mrVista-
175 elliptical”) using noise-free synthetic data. We synthesized the BOLD time series for pRFs that are
176 circular and centered at (3,3) deg, with radii spanning 0.5 - 3 deg. For these conditions, AFNI-elliptical
177 inaccurately estimates the pRFs as elongated rather than circular, whereas mrVista-elliptical estimates
178 nearly circular pRFs. We then validated the two algorithms with elliptical ground truth data (Figure 1B).
179 The ground-truth pRFs were again centered at (3,3) deg and had aspect ratios between 1.5 and 4. Again,
180 AFNI-elliptical fails to estimate the parameters accurately and mrVista-elliptical succeeds.

181

182 **Fig 1. AFNI-elliptical does not recover accurate parameters of noise-free synthetic data**

183 We analyzed noise-free synthetic data analysis with AFNI-elliptical and mrVista-elliptical. (A) AFNI-elliptical (top row) and
184 mrVista-elliptical (bottom row) analyses of circular, Gaussian, ground-truth data with four different pRF sizes. The dashed line
185 represents the 1 SD radius of the Gaussian. (B) Same as A but with elliptical ground truth data.

186

187 To explore whether there are systematic errors in AFNI-elliptical or mrVista-elliptical, we synthesized a
188 noise-free dataset by systematically varying eccentricity, size and aspect ratio (Figure 2). The AFNI-
189 elliptical algorithm generally returns incorrect aspect ratios. Over these parameter ranges, the mrVista-
190 elliptical algorithm generally returns accurate estimates.

191

192 **Fig 2. AFNI-elliptical has systematic aspect ratio errors at different eccentricities and sizes.**

193 AFNI-elliptical (top row) and mrVista (bottom row) results for circular (aspect ratio 1, solid lines) and elliptical (aspect ratio 2,
194 dashed lines) ground truth synthetic time series, with pRF radii ranging from 0.5 deg to 4 deg. *G.T.:* Ground Truth.

195 Algorithm robustness: noise analyses

196 In the presence of measurement noise, the aspect ratio of circular pRFs will be overestimated. Suppose
197 that the ground truth is a circle with radius r . The major and minor axes will both be estimates of the true
198 radius plus noise, $r + \tilde{N}$. The estimated aspect ratio, A , is the ratio of the two noisy samples constrained
199 so that the major axis is the larger of the two samples

200

$$201 \quad A = \max(r + \tilde{N}_1, r + \tilde{N}_2) / \min(r + \tilde{N}_1, r + \tilde{N}_2) \quad \text{Equation (1)}$$

202

203 From this formula we observe that (1) the estimated value must be greater than 1, and (2) the impact of
204 the noise will be large when the pRF radius is small. We performed numerical simulations of the formula
205 in Equation 1, using a range of radii and plausible noise distributions. We observed that for small radii
206 starting at 0.25 deg the median aspect ratio is of 2.5. The median aspect ratio values reduce
207 asymptotically towards the aspect ratio of 1 as the radius increases.

208

209 We tested AFNI-elliptical and mrVista-elliptical using simulated noisy datasets for a circular pRF with a
210 radius of 2 deg ([Figure 3](#)). The simulated stimulus had a TR=2, bar width of 2.8 deg and step size of 1.2
211 deg; the simulated duration was 400 seconds, including 8 bars sweeps across the visual field. The time
212 series were identical for 100 simulations except for different random samples of noise. The AFNI-
213 elliptical algorithm estimates the center location accurately, but it does not estimate the aspect ratio as
214 expected. There are many large aspect ratios (> 4), and there are many estimates of 1.0 which should be
215 rare given the noise. The mrVista-elliptical algorithm estimates the center location accurately. The
216 median aspect ratio is generally in the range between 1.2-1.4, as expected. AFNI requires the aspect ratios
217 to be bounded, so we restricted them to be between 1 and 5. MrVista has no such requirements and
218 therefore the aspect ratios were unbounded.

219

220 Based on the simulations, we expect the estimated aspect ratio of circular, noisy ground-truth data to be
221 slightly larger than 1. The mrVista-elliptical estimates conform to this expectation: they are distributed
222 compactly around an aspect ratio of 1.26 ± 0.16 (Figure 3D). The AFNI-elliptical estimates (Figure 3B)
223 are very different, with a larger mean and a much larger standard deviation: 2.07 ± 1.36 . Critically, AFNI
224 returns many aspect ratio estimates greater than 3 which suggests that such values should not be taken as
225 evidence of large aspect ratios in the data. A paired t-test comparing the magnitude of the aspect ratios
226 showed that AFNI-elliptical's error is significantly bigger than mrVista-elliptical's ($t: 6.7, p: 1.4e-09$).

227

228 **Fig 3. AFNI-elliptical estimates include large aspect ratios for circular ground-truth data with added noise.**
229 AFNI elliptical (top row) and mrVista (bottom row) analysis results for 100 noisy simulations (low noise). On the left, the
230 representation of all the receptive fields (gray) over the ground truth (blue dashed line); the black dashed line contains the center
231 locations and the blue dashed line represents the 1 SD radius of the Gaussian. On the right, the histogram of the aspect ratios. The
232 median is indicated by the red line. SNR is the mean and STD of all 100 bold time series. Due to differences in the HRFs
233 between the two algorithms and randomization used in the synthesis, the average SNR of the simulated time series differs, being
234 lower for mrVista.

235

236 To test the generality of these findings, we synthesized and analyzed ground truth datasets with a broader
237 range of parameters. For AFNI-elliptical (Figure 4), the estimated aspect ratio for circular pRFs was about
238 2.5-3.0 for all ground truth radii (Figure 4A). The distribution of values is quite wide, spanning all the
239 aspect ratios within the 1,5 bounds (Figure 4B). When the ground-truth aspect ratio was 2, the estimated
240 aspect ratio increased to a median value of 4, but the distribution remained very broad. These simulations
241 used the mid-level of noise (see Methods). The results were similar for the low-level noise, and various
242 eccentricity values. These validation tests reveal that, with our configuration, environment variables and
243 function calls, AFNI-elliptical is not a suitable tool for assessing the aspect ratio of population receptive
244 fields. The validation tests produce a wide range of aspect ratio distributions, as found in the empirical
245 analyses reported by Silson et al. (2018). The reason for the differences in these AFNI distributions is
246 unknown.

247

248 **Fig 4. AFNI-elliptical does not estimate the correct aspect ratio of synthetic data.**

249 (A) Estimated aspect ratio (ground truth aspect ratio = 1) as a function of pRF radius (deg). The points are the median and the
250 lines show the range corresponding to the central 50% of the estimates. (B) Histogram of estimated aspect ratios (ground truth
251 aspect ratio = 1) using simulated pRFs with a mixture of radius sizes (1-4 deg) and eccentricities (2-6 deg). (C) Histogram of
252 estimated aspect ratios (ground truth aspect ratio = 2) for the same mixture of radius sizes and eccentricities. The simulated bar
253 width is 2.8 deg and the bar translates 1.2 deg for each TR (2 sec). The simulations used the mid-level of noise. The red arrow
254 indicates the median value of the histogram. *G.T.: Ground Truth.*

255

256 We next analyzed the ability of mrVista-elliptical to accurately estimate the pRF aspect ratio (Figure 5).
257 As expected from the basic analysis of signal to noise (Equation 1), the accuracy of the aspect ratio
258 estimates depends on pRF size and properties of the stimulus. With a TR of 2 s, simulations with small
259 pRF radius (~1 deg or less) are very inaccurate, including many large aspect ratios (Figure 5A). We
260 simulated the accuracy of recovering a circular pRF using a mixture of pRF sizes (1-4 deg) and
261 eccentricities (2-6 deg). The median estimated aspect ratio is approximately 1.5, with the estimates falling
262 mostly between 1 and 2 (Figure 5B). Simulating with a ground-truth aspect ratio of 2 increases the
263 median, but the estimates are spread over a large range (Figure 5C).

264

265 To understand how empirical methods using mrVista might impact algorithm validity, we carried out
266 simulations with different experimental parameters. Specifically, we simulated an experimental protocol
267 with a shorter TR (1 s instead of 2 s), corresponding to a smaller stimulus step size. The mrVista-elliptical
268 estimates are more accurate over a larger range (Figure 5D). Estimating ground-truth pRFs with a range
269 of sizes and eccentricities, the median aspect ratio is 1.25 and the range is more compact (Figure 5E).
270 The estimates for a ground truth aspect ratio of 2 and multiple pRF sizes have a median aspect ratio
271 slightly larger than 2 (2.2). The same analysis performed with a 2-s TR and low noise results in estimates
272 similar to the 1-s TR simulations.

273

274 Fig 5. mrVista-elliptical aspect ratio estimates are close to accurate over a limited range of conditions.
275 (A) Estimated aspect ratio (ground truth = 1) as a function of pRF radius (deg). The points are the median and the lines show the
276 range corresponding to 50% of the estimates. (B) Histogram of estimated aspect ratios (ground truth = 1) using simulated pRFs
277 with a mixture of radius sizes (1-4 deg) and eccentricities (2-6 deg). (C) Histogram of estimated aspect ratios (ground truth = 2)
278 for the same mixture of radius sizes and eccentricities. The simulated bar width is 2.8 deg and the bar translates 1.2 deg for each
279 TR (2 sec). The simulations used the mid-level of noise. (D-F) The same graphs calculated with a smaller bar displacement (0.6
280 deg) and shorter TR (1 sec). For the large bar step size the mrVista elliptical estimates differ between the ground-truth aspect
281 ratios of 1 and 2, although there is very poor accuracy when the ground truth aspect ratio is 2. Reducing the bar step size and
282 increasing the number of temporal samples improves the accuracy of the aspect ratio estimate (D-F). The peaks in the histogram
283 at aspect ratios of 1.25, 1.6 and 2.5 in B, E are a flaw in the algorithm. These peaks, which are present in fits to empirical data
284 (below), are likely due to the coarse-to-fine search method implemented in the algorithm. These simulations define a range of
285 experimental parameters where mrVista-elliptical provides useful information about the aspect ratio. *G.T.: Ground Truth.*

286

287 The mrVista-elliptical algorithm has a numerical estimation error that biases the results to return certain
288 aspect ratios (1.25, 1.65, 2.5); these are the peaks in the histogram. We suspect this failure arises from the
289 multi-resolution (coarse to fine) search methodology. The coarse fit uses a grid of parameter values, and
290 the values of the aspect ratio in the grid include these three values. This limitation of the algorithm does
291 not render it unusable for further exploration with real measurements under certain conditions.

292 Empirical measurement: estimated aspect ratio

293 We used mrVista-elliptical and experimental data to assess the aspect ratio of pRFs in early visual cortex.
294 We analyzed three typical subjects from the HCP 7T retinotopy dataset (Benson et al., 2018). We first
295 used mrVista-circular to assess the parameter ranges. The estimated range of eccentricity values (2.5-6.5
296 degs) and the pRF areas (6.5-30 deg²) were then used to restrict the mrVista-elliptical fits. These
297 parameters are consistent with many previous estimates and place no restriction on the estimated aspect
298 ratio values. The HCP dataset was acquired with a TR of 1 s and a duration of 300 secs, and our analysis
299 of synthetic data above indicates that in this spatial step, eccentricity and size range, the median mrVista-

300 elliptical aspect ratios are reliable. Each subject had two runs with sweeping bar stimuli, and we analyzed
301 the average of these runs.

302

303 We also created synthetic datasets with low- and mid-noise levels to compare with the experimental data
304 (Figure 6). The synthetic datasets used the same sequence of stimulus apertures as the experimental data.

305

306 The analyses of the experimental data returned a median pRF aspect ratio of about 1.5, with no systematic
307 effects of ventral vs dorsal, or eccentricity (Figure 6A). The values are slightly larger in V1. There is no
308 significant trend in the aspect ratio as a function of eccentricity. The aspect ratio from the experimental
309 data is similar to the ratio in the mid-noise synthetic data. The experimental data aspect-ratios have higher
310 variance than the synthetic values, but they are within the 95% confidence interval of the mid-noise
311 synthetic aspect ratio estimations. As expected, the low-noise synthetic data simulations have aspect
312 ratios closer to the ground truth value. This indicates that the mid-noise level of the synthetic data is a
313 good approximation to the experimental data (Figure 6B). When comparing experimental data from all
314 maps, the histograms are similar, with median aspect ratio values at around 1.5. The validation procedures
315 (Figure 5) show that mrVista can accurately capture aspect ratios of 2, and yet the empirical data return a
316 distribution of aspect ratios that is smaller, closer to the theoretically expected values of a circular ground
317 truth.

318

319 Finally, we analyzed the strength of the evidence in favor of using an elliptical model compared to the
320 circular model. The elliptical model uses two more parameters and contains the circular model as a
321 special case. Hence, it is expected that the variance explained (R^2) will be higher for the elliptical model.
322 In rare cases, the R^2 is lower for the elliptical model, indicating a failure of the optimization to find the
323 best solution. Figure 6C shows the histogram of the difference between the R^2 of the elliptical and circular
324 fits, for all experimental data in which the models explain more than 25% of the variance. The elliptical

Circular vs elliptical pRFs

325 fit is systematically higher than the circular fit, but the median difference is less than 1%, and even the
326 few voxels with the largest difference are no more than 5%. Hence, there is almost no evidence in support
327 of using the elliptical model over the circular model for these experimental data. Detecting differences
328 from circularity will require new protocols and models.

329

330 **Fig 6. mrVista-elliptical pRF parameters estimated from empirical measurements in V1-3 (N=3).**

331 (A) Estimated median pRF aspect ratios of experimental (color) data plotted as a function of eccentricity. The experimental data
332 are plotted separately for ventral and dorsal regions of V1-3. Synthetic data were created using mid-level noise and are
333 represented as a light gray band containing the central 95% aspect ratio values. The experimental data aspect-ratio fits show a
334 large variance across voxels, but except one case, the population medians are within the expected range of the (mid) noise
335 simulations. (B) Histograms of the estimated pRF aspect ratio for experimental (gray) and synthetic (black) data. Estimates were
336 included in the histograms if the model fit explained at least 25% of the variance and the pRF position was between 2.5-6.5 deg
337 and the pRF area size estimate was between 6.5-30 deg². The ground truth aspect ratio for the synthetic data was 1. The thin
338 dashed vertical lines represent the median values for the experimental and synthetic analyses. (C) Histogram of the difference in
339 variance explained (R^2) between the elliptical and circular model fits to the experimental data. The histogram includes data
340 subject to the same restrictions as in (B). The precise parameters for determining the restriction do not impact the conclusions in
341 either (B) or (C).

342

343 Many analyses of these types of histograms, separating the data in various ways such as dorsal and ventral
344 or by visual field map, support the same conclusions. The median aspect ratio values remain between 1.25
345 and 1.5, and we found no systematic relationship between the estimated aspect ratio or ellipse orientation
346 and pRF position in the visual field.

347 Discussion

348 The application of pRF methods

349 Multiple groups have used population receptive field parameters as dependent variables to understand the
350 effects of cortical plasticity, attention, and diagnostic tools for neurology and psychiatry (Wandell and
351 Winawer, 2015). For example, pRF methods have been used to examine hypotheses about brain substrate
352 changes, such as excitation-inhibition imbalances, that may be associated with neurological,
353 ophthalmologic and psychiatric diseases (Papanikolaou et al., 2014; Wandell and Winawer, 2015;
354 Anderson et al., 2017; Dumoulin and Knapen, 2018). There are also opportunities to understand
355 individual differences in the visual pathways that may impact performance in tasks that rely on vision,
356 such as reading (Le et al., 2017) and face recognition (Witthoft et al., 2016). Establishing the precision of
357 the parameter estimates obtained with current protocols and tools enables us to determine with more
358 confidence whether an individual under study is within the distribution of typical subjects.

359 Oriented pRFs

360 What would be a plausible biological basis for pRFs with large aspect ratios? Many neurons in primary
361 visual cortex have oriented receptive fields. For simple cells, the spatial envelope tends to be elongated
362 along the axis of orientation tuning (De Valois et al., 1982; Ringach, 2002; Michel et al., 2013). The
363 neurons are arranged in an orderly pattern such that the main orientation changes smoothly across the
364 cortical surface. The receptive fields span many orientations over a 1 mm distance (Hubel and Wiesel,
365 1974). In typical 3T measurements, a single fMRI voxel aggregates the response over a millimeter or
366 more and thus accumulates the metabolic response from neurons with many orientations. It would be
367 quite surprising if the orientation of neuronal receptive fields could be observed robustly in functional
368 MRI measurements. Although there have been some claims to this effect (Kamitani and Tong, 2005;

369 Sasaki et al., 2006; Freeman et al., 2011), it appears now that these biases are due to properties of the
370 stimulus aperture rather than to orientation tuning (Carlson, 2014; Roth et al., 2018)

371

372 Alternatively, the pRF from a voxel could be elongated if the neural RFs center positions within a voxel
373 had an asymmetric distribution. Such asymmetric distributions might occur if, for example, the cortical
374 magnification differed systematically between the radial and tangential directions. The effect of neural RF
375 distribution within a voxel on the shape of the pRF is, however, likely to be modest (Amano et al., 2009).
376 Were the pRF measurements truly to have a large aspect ratio, we would still need to find a plausible
377 biological basis.

378

379 We are unaware of claims other than Silson et al. (2018) that one can reliably measure a large aspect ratio
380 based on the fMRI response from individual voxels. Direct comparisons of standard pRF models suggest
381 that circular receptive field models provide the best fits (Zeidman et al., 2018; Figure 10). Using novel
382 measurement approaches, investigators report that individual fMRI voxels may have some orientation
383 preference with a magnitude similar to the values reported here (Greene et al., 2014; Merkel et al., 2018,
384 2020).

385

386 For example, Merkel et al. (2018; 2020) estimated the aspect ratios of voxels in early visual cortex and
387 reported ellipticity (the inverse of aspect ratio) ranging between 0.6 and 1, which corresponds to aspect
388 ratios of 1 to 1.67 (Figure 7A; Merkel et al., 2020). Using tomographic methods to estimate pRF shapes
389 (Greene et al., 2014) also estimated aspect ratios (Figure 7B). The distribution they report had 11% of the
390 aspect ratios greater than 2 which is close to the expected amount based on our simulations with synthetic
391 data assuming circular pRFs (14%) and based on analysis with the HCP 7T (8%) data.

392

393 **Fig 7. Ellipticity results reported in the literature show similar results to our circular ground truth simulations**

394 (A) Ellipticity (1/Aspect Ratio) reported in (Merkel et al., 2020). (B) Aspect ratio reported in (Greene et al., 2014).

395

396 These aspect ratios are not meaningfully different from circular given the expected level of experimental
397 noise and current protocols. Specifically, by definition the estimated aspect ratio value must exceed 1.
398 Further, the impact of experimental noise will be quite large when the pRF radius is small. For example,
399 using 0.7 deg standard deviations as noise, for small radii (0.25 - 1 deg) the expected median aspect ratio
400 is almost 3. This value reduces asymptotically towards the aspect ratio of 1 for large pRF sizes (> 5 deg).
401 Moreover, pRF size estimates are less robust than pRF center estimates and the absolute value depends
402 strongly on the individual HRFs (Lage-Castellanos et al., 2020; Lerma-Usabiaga et al., 2020).

403

404 These principles and simulations show accurate estimation of aspect ratio values as small as 1.5 will
405 require new experimental paradigms that mitigate instrumental noise and account for the computational
406 uncertainties. It would also be preferable to use methods that include an accurate assessment of the
407 individual subject's HRF. Elsewhere we used simulations to describe adjustments to experimental
408 protocols that should improve the accuracy and stability of pRF measurements (Lerma-Usabiaga et al.,
409 2020). Implementing and validating these methods will require some patience.

410 Conclusion

411 This project began with a report that the aspect ratios of pRFs in early visual cortex are substantially
412 larger than previously thought (Silson et al., 2018). We set out to investigate this report, and we
413 concluded that the difference could be traced to a software implementation. Our new data analysis
414 confirmed the prior consensus about pRF shapes in early visual cortex: the best-fitting shapes are not very
415 different from circular (Greene et al., 2014; Zeidman et al., 2018; Merkel et al., 2020). The ability to
416 measure shapes with greater precision, perhaps revealing systematic deviations at individual voxels or
417 even orientation maps, will require advances in protocols and analyses. Simulations suggest these may be
418 in reach (Figure 5).

419

420 The complexity of modern neuroimaging analyses has arrived at a point where explicit and public
421 validation frameworks are important for building trust in publications and as part of the standard for
422 software distribution. Here, we used the validation framework implemented in (Lerma-Usabiaga et al.,
423 2020). The development of validated models and quantified parameter estimates has been a hallmark of
424 sensory science, and we continue that approach here.

425 References

- 426 Alvarez I, de Haas B, Clark CA, Rees G, Schwarzkopf DS (2015) Comparing different stimulus
427 configurations for population receptive field mapping in human fMRI. *Front Hum Neurosci* 9:96.
- 428 Amano K, Wandell B a., Dumoulin SO (2009) Visual field maps, population receptive field sizes, and
429 visual field coverage in the human MT+ complex. *J Neurophysiol* 102:2704–2718.
- 430 Anderson EJ, Tibber MS, Sam Schwarzkopf D, Shergill SS, Fernandez-Egea E, Rees G, Dakin SC (2017)
431 Visual Population Receptive Fields in People with Schizophrenia Have Reduced Inhibitory
432 Surrounds. *The Journal of Neuroscience* 37:1546–1556 Available at:
433 <http://dx.doi.org/10.1523/jneurosci.3620-15.2016>.
- 434 Benson NC, Jamison KW, Arcaro MJ, Vu AT, Glasser MF, Coalson TS, Van Essen DC, Yacoub E,
435 Ugurbil K, Winawer J, Kay K (2018) The Human Connectome Project 7 Tesla retinotopy dataset:
436 Description and population receptive field analysis. *J Vis* 18:23.
- 437 Carlson TA (2014) Orientation decoding in human visual cortex: new insights from an unbiased
438 perspective. *J Neurosci* 34:8373–8383.
- 439 Cox RW (1996) AFNI: software for analysis and visualization of functional magnetic resonance

- 440 neuroimages. *Comput Biomed Res* 29:162–173.
- 441 De Valois RL, Albrecht DG, Thorell LG (1982) Spatial frequency selectivity of cells in macaque visual
442 cortex. *Vision Res* 22:545–559.
- 443 Dumoulin SO, Knapen T (2018) How Visual Cortical Organization Is Altered by Ophthalmologic and
444 Neurologic Disorders. *Annual Review of Vision Science* 4:357–379 Available at:
445 <http://dx.doi.org/10.1146/annurev-vision-091517-033948>.
- 446 Dumoulin SO, Wandell B a. (2008) Population receptive field estimates in human visual cortex.
447 *Neuroimage* 39:647–660.
- 448 Freeman J, Brouwer GJ, Heeger DJ, Merriam EP (2011) Orientation decoding depends on maps, not
449 columns. *J Neurosci* 31:4792–4804.
- 450 Greene CA, Dumoulin SO, Harvey BM, Ress D (2014) Measurement of population receptive fields in
451 human early visual cortex using back-projection tomography. *J Vis* 14 Available at:
452 <http://dx.doi.org/10.1167/14.1.17>.
- 453 Hubel DH, Wiesel TN (1968) Receptive fields and functional architecture of monkey striate cortex. *J*
454 *Physiol* 195:215–243.
- 455 Hubel DH, Wiesel TN (1974) Uniformity of monkey striate cortex: a parallel relationship between field
456 size, scatter, and magnification factor. *J Comp Neurol* 158:295–305.
- 457 Kalatsky VA, Stryker MP (2003) New Paradigm for Optical Neurotechnique Imaging: Temporally
458 Encoded Maps of Intrinsic Signal. *Neuron* 38:529–545.
- 459 Kamitani Y, Tong F (2005) Decoding the visual and subjective contents of the human brain. *Nat Neurosci*
460 8:679–685.

- 461 Kay KN, Winawer J, Mezer A, Wandell BA (2013) Compressive spatial summation in human visual
462 cortex. *J Neurophysiol* 110:481–494.
- 463 Lage-Castellanos A, Valente G, Senden M, De Martino F (2020) Investigating the Reliability of
464 Population Receptive Field Size Estimates Using fMRI. *Front Neurosci* 14:825.
- 465 Lerma-Usabiaga G, Benson N, Winawer J, Wandell BA (2020) A validation framework for neuroimaging
466 software: The case of population receptive fields. *PLoS Comput Biol* 16:e1007924.
- 467 Le R, Witthoft N, Ben-Shachar M, Wandell B (2017) The field of view available to the ventral occipito-
468 temporal reading circuitry. *J Vis* 17:6.
- 469 Merkel C, Hopf J-M, Schoenfeld MA (2020) Modulating the global orientation bias of the visual system
470 changes population receptive field elongations. *Hum Brain Mapp* 41:1765–1774.
- 471 Merkel C, Hopf J, Schoenfeld MA (2018) Spatial elongation of population receptive field profiles
472 revealed by model-free fMRI back-projection. *Hum Brain Mapp* 39:2472–2481.
- 473 Michel MM, Chen Y, Geisler WS, Seidemann E (2013) An illusion predicted by V1 population activity
474 implicates cortical topography in shape perception. *Nat Neurosci* 16:1477–1483.
- 475 Nauhaus I, Nielsen KJ, Callaway EM (2016) Efficient Receptive Field Tiling in Primate V1. *Neuron*
476 91:893–904.
- 477 Papanikolaou A, Keliris GA, Papageorgiou TD, Shao Y, Krapp E, Papageorgiou E, Stingl K, Bruckmann
478 A, Schiefer U, Logothetis NK, Smirnakis SM (2014) Population receptive field analysis of the
479 primary visual cortex complements perimetry in patients with homonymous visual field defects. *Proc*
480 *Natl Acad Sci U S A* 111:E1656–E1665.
- 481 Ringach DL (2002) Spatial structure and symmetry of simple-cell receptive fields in macaque primary
482 visual cortex. *J Neurophysiol* 88:455–463.

- 483 Roth Z, Heeger D, Merriam E (2018) Orientation selectivity and stimulus vignetting in human visual
484 cortex. 2018 Conference on Cognitive Computational Neuroscience Available at:
485 <http://dx.doi.org/10.32470/ccn.2018.1245-0>.
- 486 Sasaki Y, Rajimehr R, Kim BW, Ekstrom LB, Vanduffel W, Tootell RBH (2006) The Radial Bias: A
487 Different Slant on Visual Orientation Sensitivity in Human and Nonhuman Primates. *Neuron*
488 51:661–670 Available at: <http://dx.doi.org/10.1016/j.neuron.2006.07.021>.
- 489 Silson EH, Reynolds RC, Kravitz DJ, Baker CI (2018) Differential Sampling of Visual Space in Ventral
490 and Dorsal Early Visual Cortex. *J Neurosci* 38:2294–2303.
- 491 Wandell BA, Winawer J (2015) Computational neuroimaging and population receptive fields. *Trends*
492 *Cogn Sci* 19:349–357.
- 493 Witthoft N, Poltoratski S, Nguyen M, Golarai G, Liberman A, LaRocque KF, Smith ME, Grill-Spector K
494 (2016) Reduced spatial integration in the ventral visual cortex underlies face recognition deficits in
495 developmental prosopagnosia. :051102 Available at:
496 <https://www.biorxiv.org/content/10.1101/051102v1> [Accessed September 2, 2020].
- 497 Zeidman P, Silson EH, Schwarzkopf DS, Baker CI, Penny W (2018) Bayesian population receptive field
498 modelling. *Neuroimage* 180:173–187.
- 499 Zuiderbaan W, Harvey BM, Dumoulin SO (2012) Modeling center–surround configurations in population
500 receptive fields using fMRI. *J Vis* 12:10–10.

501

502

503 Legends

504 **Fig 1. AFNI-elliptical does not recover accurate parameters of noise-free synthetic data**505 We analyzed noise-free synthetic data analysis with AFNI-elliptical and mrVista-elliptical. (A) AFNI-elliptical (top row) and
506 mrVista-elliptical (bottom row) analyses of circular, Gaussian, ground-truth data with four different pRF sizes. The dashed line
507 represents the 1 SD radius of the Gaussian. (B) Same as A but with elliptical ground truth data.508
509 **Fig 2. AFNI-elliptical has systematic aspect ratio errors at different eccentricities and sizes.**510 AFNI-elliptical (top row) and mrVista (bottom row) results for circular (aspect ratio 1, solid lines) and elliptical (aspect ratio 2,
511 dashed lines) ground truth synthetic time series, with pRF radii ranging from 0.5 deg to 4 deg. *G.T.: Ground Truth.*512
513 **Fig 3. AFNI-elliptical estimates include large aspect ratios for circular ground-truth data with added noise.**514 AFNI elliptical (top row) and mrVista (bottom row) analysis results for 100 noisy simulations (low noise). On the left, the
515 representation of all the receptive fields (gray) over the ground truth (blue dashed line); the black dashed line contains the center
516 locations and the blue dashed line represents the 1 SD radius of the Gaussian. On the right, the histogram of the aspect ratios.
517 The median is indicated by the red line. SNR is the mean and STD of all 100 bold time series. Due to differences in the HRFs
518 between the two algorithms and randomization used in the synthesis, the average SNR of the simulated time series differs, being
519 lower for mrVista.520
521 **Fig 4. AFNI-elliptical does not estimate the correct aspect ratio of synthetic data.**522 (A) Estimated aspect ratio (ground truth aspect ratio = 1) as a function of pRF radius (deg). The points are the median and the
523 lines show the range corresponding to the central 50% of the estimates. (B) Histogram of estimated aspect ratios (ground truth
524 aspect ratio = 1) using simulated pRFs with a mixture of radius sizes (1-4 deg) and eccentricities (2-6 deg). (C) Histogram of
525 estimated aspect ratios (ground truth aspect ratio = 2) for the same mixture of radius sizes and eccentricities. The simulated bar
526 width is 2.8 deg and the bar translates 1.2 deg for each TR (2 sec). The simulations used the mid-level of noise. The red arrow
527 indicates the median value of the histogram. *G.T.: Ground Truth.*528
529 **Fig 5. mrVista-elliptical aspect ratio estimates are close to accurate over a limited range of conditions.**530 (A) Estimated aspect ratio (ground truth = 1) as a function of pRF radius (deg). The points are the median and the lines show the
531 range corresponding to 50% of the estimates. (B) Histogram of estimated aspect ratios (ground truth = 1) using simulated pRFs
532 with a mixture of radius sizes (1-4 deg) and eccentricities (2-6 deg). (C) Histogram of estimated aspect ratios (ground truth = 2)
533 for the same mixture of radius sizes and eccentricities. The simulated bar width is 2.8 deg and the bar translates 1.2 deg for each
534 TR (2 sec). The simulations used the mid-level of noise. (D-F) The same graphs calculated with a smaller bar displacement (0.6
535 deg) and shorter TR (1 sec). For the large bar step size the mrVista elliptical estimates differ between the ground-truth aspect
536 ratios of 1 and 2, although there is very poor accuracy when the ground truth aspect ratio is 2. Reducing the bar step size and
537 increasing the number of temporal samples improves the accuracy of the aspect ratio estimate (D-F). The peaks in the histogram
538 at aspect ratios of 1.25, 1.6 and 2.5 in B, E are a flaw in the algorithm. These peaks, which are present in fits to empirical data
539 (below), are likely due to the coarse-to-fine search method implemented in the algorithm. These simulations define a range of
540 experimental parameters where mrVista-elliptical provides useful information about the aspect ratio. *G.T.: Ground Truth.*541
542 **Fig 6. mrVista-elliptical pRF parameters estimated from empirical measurements in V1-3 (N=3).**543 (A) Estimated median pRF aspect ratios of experimental (color) data plotted as a function of eccentricity. The experimental data
544 are plotted separately for ventral and dorsal regions of V1-3. Synthetic data were created using mid-level noise and are
545 represented as a light gray band containing the central 95% aspect ratio values. The experimental data aspect-ratio fits show a
546 large variance across voxels, but except one case, the population medians are within the expected range of the (mid) noise
547 simulations. (B) Histograms of the estimated pRF aspect ratio for experimental (gray) and synthetic (black) data. Estimates were
548 included in the histograms if the model fit explained at least 25% of the variance and the pRF position was between 2.5-6.5 deg
549 and the pRF area size estimate was between 6.5-30 deg². The ground truth aspect ratio for the synthetic data was 1. The thin
550 dashed vertical lines represent the median values for the experimental and synthetic analyses. (C) Histogram of the difference in
551 variance explained (R^2) between the elliptical and circular model fits to the experimental data. The histogram includes data
552 subject to the same restrictions as in (B). The precise parameters for determining the restriction do not impact the conclusions in
553 either (B) or (C).554
555 **Fig 7. Ellipticity results reported in the literature show similar results to our circular ground truth simulations**

556 (A) Ellipticity (1/Aspect Ratio) reported in (Merkel et al., 2020). (B) Aspect ratio reported in (Greene et al., 2014).

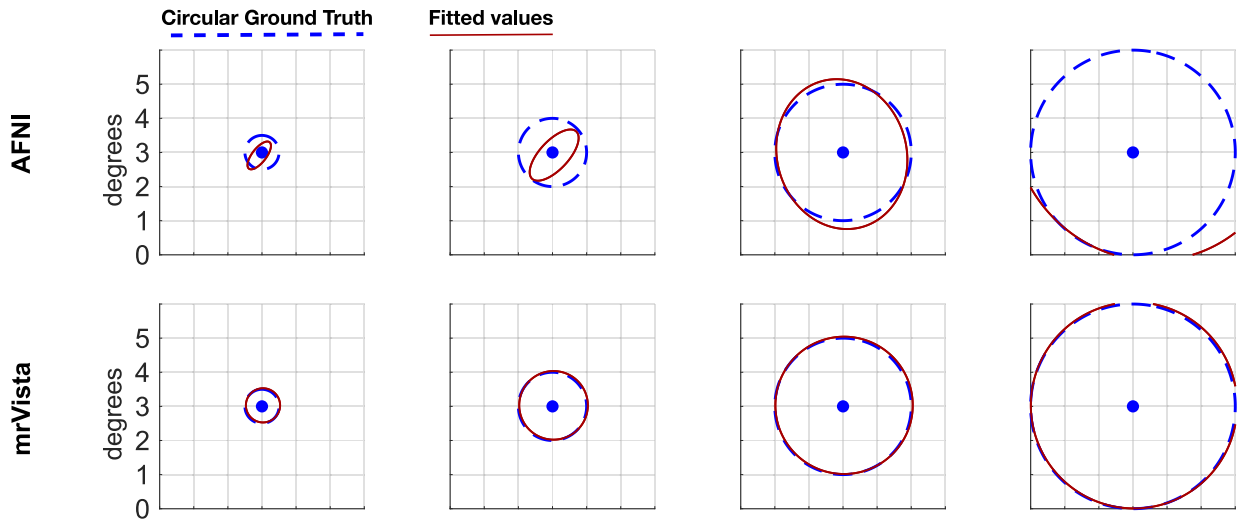
557

558 **Table 1. Main parameters of the experiments**

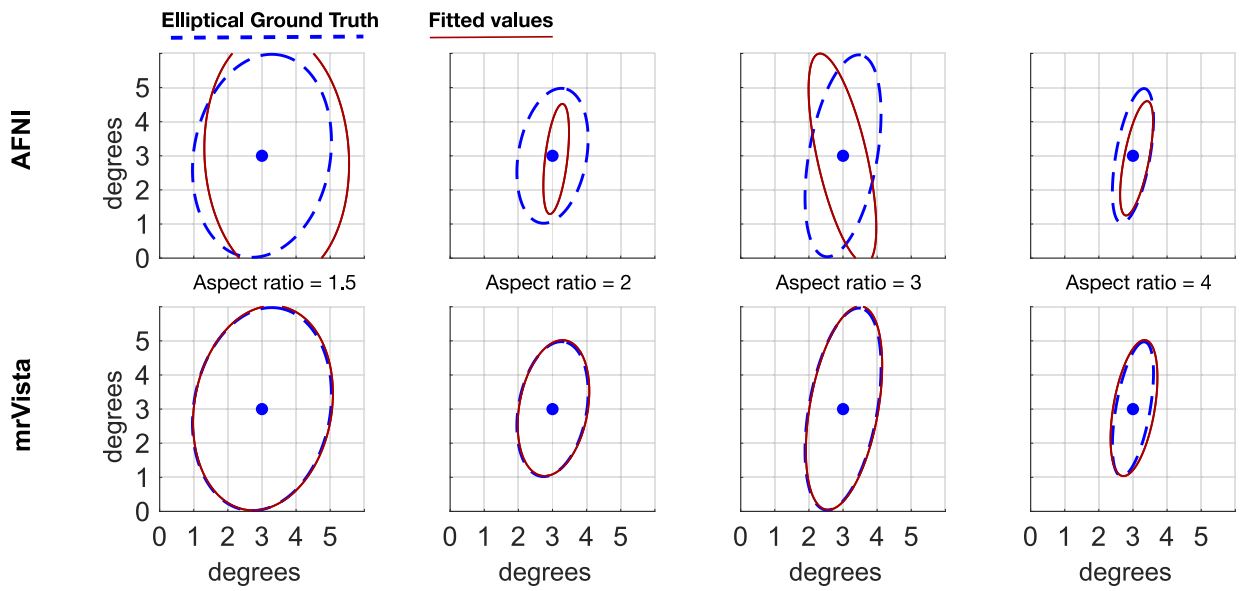
559 ** Note: 6 refers to the elliptical fits with 6 parameters, and 4 to the circular fits with 4 parameters.*

560

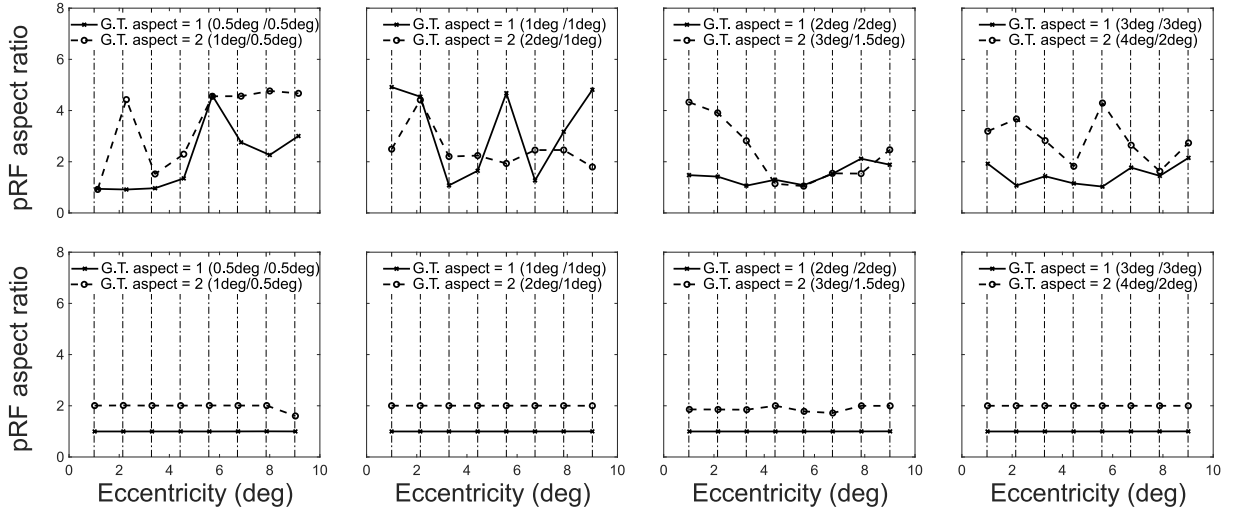
A

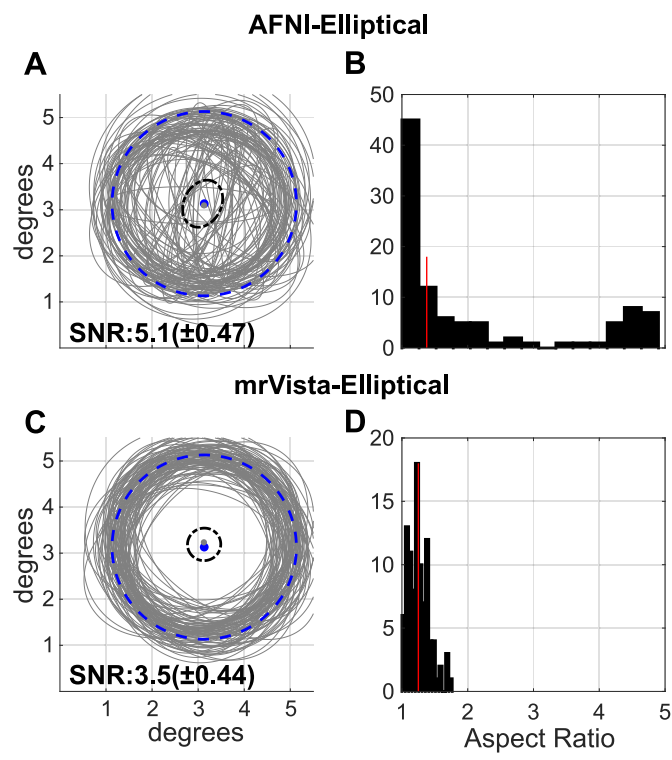


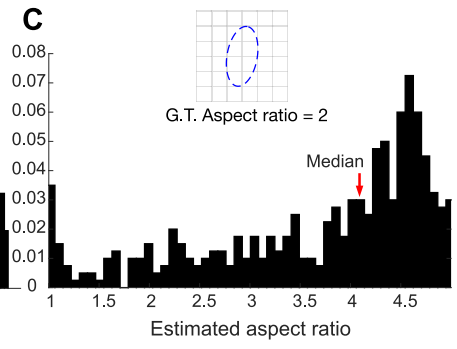
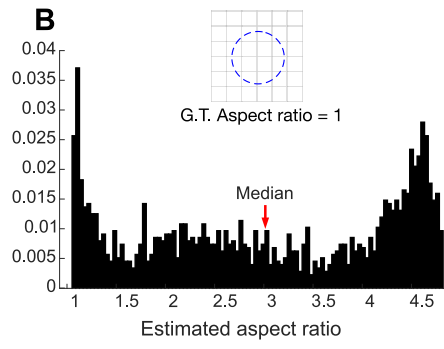
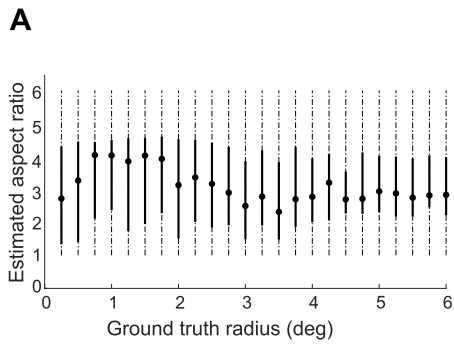
B



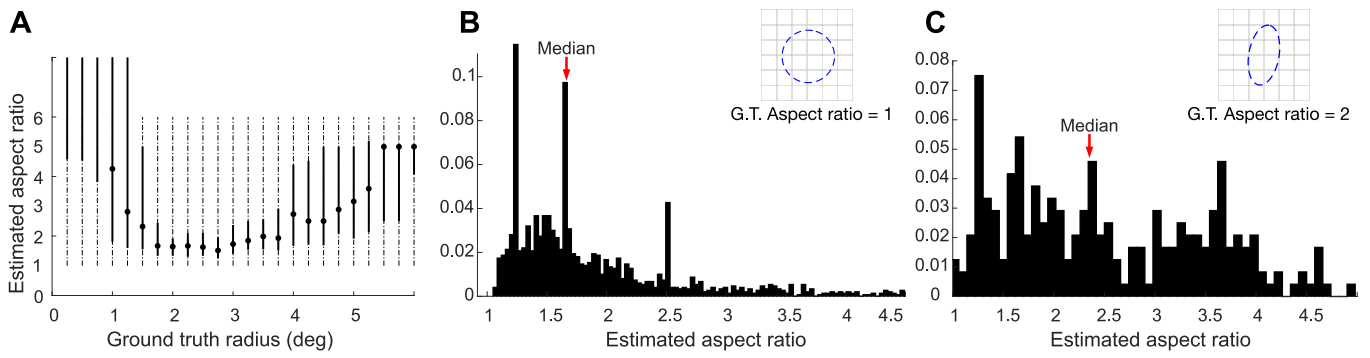
AFNI







TR = 2 s.



TR = 1 s.

